


RESEARCH

Open Access



Natural diversity of glycoside hydrolase family 48 exoglucanases: insights from structure

Roman Brunecky¹, Markus Alahuhta¹, Deanne W. Sammond¹, Qi Xu¹, Mo Chen², David B. Wilson^{3^}, John W. Brady², Michael E. Himmel¹, Yannick J. Bomble^{1*}  and Vladimir V. Lunin^{1*}

Abstract

Glycoside hydrolase (GH) family 48 is an understudied and increasingly important exoglucanase family found in the majority of bacterial cellulase systems. Moreover, many thermophilic enzyme systems contain GH48 enzymes. Deletion of GH48 enzymes in these microorganisms results in drastic reduction in biomass deconstruction. Surprisingly, given their importance for these microorganisms, GH48s have intrinsically low cellulolytic activity but even in low ratios synergize greatly with GH9 endoglucanases. In this study, we explore the structural and enzymatic diversity of these enzymes across a wide range of temperature optima. We have crystallized one new GH48 module from *Bacillus pumilus* in a complex with cellobiose and cellohexaose (*BpumGH48*). We compare this structure to other known GH48 enzymes in an attempt to understand GH48 structure/function relationships and draw general rules correlating amino acid sequences and secondary structures to thermostability in this GH family.

Keywords: GH48, Circular dichroism, X-ray crystallography, Cellulase, Molecular modeling

Background

Enzymes in the glycoside hydrolase family 48 are believed to be an important member of many bacterial cellulase systems which also lack the better studied GH6 and GH7 family cellobiohydrolases produced by most cellulolytic fungi [1]. According to the CAZy database, family GH48 consists of 937 known enzymes, 903 of which are from bacterial organisms [2]. The most studied GH48 enzymes are GH48a from *Thermobifida fusca*, the cellulosomal GH48 CelS, and the non-cellulosomal GH48 CelY from *Clostridium thermocellum* [3–7]. Many GH48 enzymes are also produced by thermophilic and hyperthermophilic species, some of them being considered strong candidates for consolidated bioprocessing, making them attractive to study for potential applications in the nascent biofuels industry within thermal tolerant cellulase commercial preparations or consolidated Bioprocessing (CBP) applications. However, for a long time, there were only two protein structures deposited in the protein data bank (PDB) for this family

of glycoside hydrolases making structure/function studies complicated. Recently, five more structures of family 48 glycoside hydrolases were deposited to the PDB, bringing the total number of known structures to seven. To broaden the structural database and directly correlate activity to structural features, we have characterized and expressed two GH48 domains from *C. bescii* and *B. pumilus* and solved their structures using X-ray crystallography. We have also determined the melting temperatures for these enzymes and determined their activity levels using phosphoric acid swollen cellulose (PASC) and bacterial microcrystalline cellulose (BMCC). We have selected five of these available PDB structures, used structural informatics and protein modeling approaches to identify features that may explain the observed thermostability variation in this family; as well the similar activity levels observed for these enzymes.

Results and discussion

Differences in stability but not in cellulolytic activity

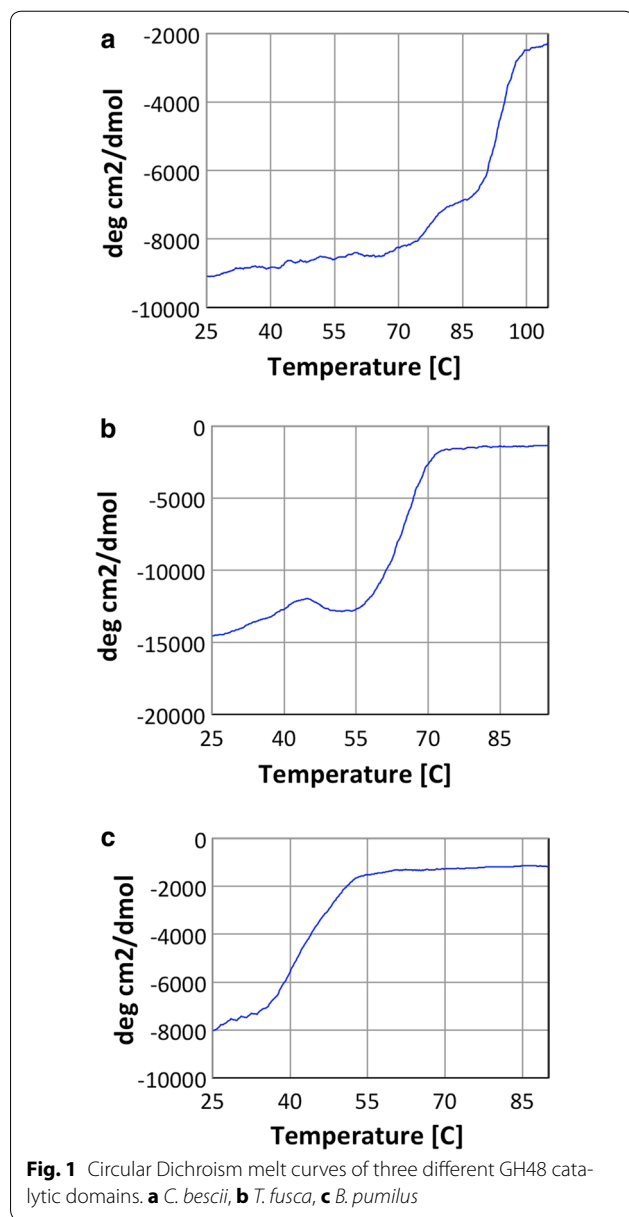
Circular dichroism spectroscopy was used to determine the melting temperature of each enzyme. The melting temperatures for purified GH48 enzymes isolated from *C. bescii*, *T. fusca*, and *B. pumilus*, were determined to be 80, 65, and 45 °C, respectively (Fig. 1). The wide range

*Correspondence: yannick.bomble@nrel.gov; Vladimir.Lunin@nrel.gov

[^] Deceased

¹ Biosciences Center, National Renewable Energy Laboratory, 15013 Denver West Parkway, Golden, CO 80401, USA

Full list of author information is available at the end of the article



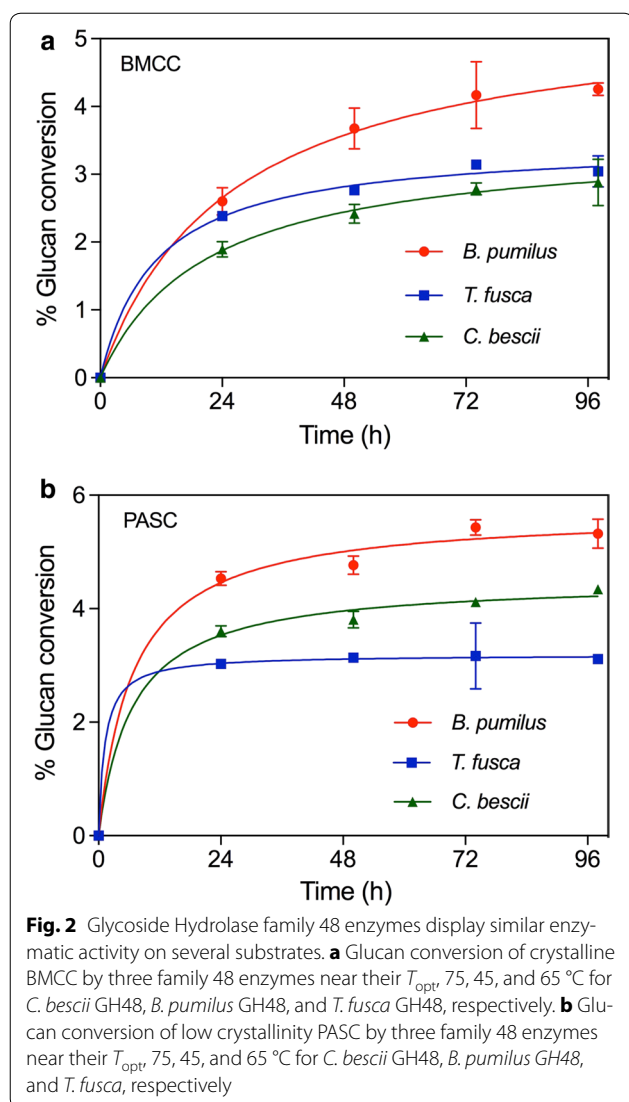
of melting temperatures for these constructs provides a range from thermophilic to mesophilic and it is interesting to note that the sequence identity for all these GH48 modules is high (between 46 and 62%) (see Table 1 and Additional file 1: Figure S1)—despite a 35 °C range in melting temperature for the enzymes. All the melting temperatures are as expected higher than the optimal growth temperatures of the host organism but not by a large margin.

The results of the enzyme digestions are shown in Fig. 2a, b. It is somewhat surprising that there is very little difference in the extent of conversion displayed by these enzymes considering the 35 °C difference in their temperature optima. The *B. pumilus* GH48 seems to outperform the other two GH48 enzymes by a small margin all at their optimal operating temperatures. Furthermore, it is also somewhat surprising that there is no apparent preference by these enzymes for neither the low crystallinity phosphoric acid swollen cellulose (PASC) substrate nor the more crystalline, bacterial microcrystalline cellulose (BMCC) substrate. It should be noted that low overall extents of conversion on insoluble substrates are typical for GH48 exoglucanases and can be improved with the addition of GH9 endoglucanases [7]. However, we would expect that the CelA GH48 from *C. bescii* would have the highest activity on cellulose based on both the high activity of this multi-modular enzyme and its much higher thermostability; whereas we would expect the *B. pumilus* GH48 to have significantly lower activity based on its much lower temperature optimum [10]. With regard to the *T. fusca* GH48, we would expect to find an intermediate level of activity based on its intermediate thermostability and previously reported activity measurements [7]. However, this result was not found in this study. When the enzymes are run at their temperature optima, we found that the *B. pumilus* GH48 seems slightly more active when compared to the other two enzymes under these conditions on both the crystalline and amorphous substrates tested (Fig. 2a, b).

Table 1 Characteristics of select glycoside hydrolase family 48 enzymes

PDB	Organism	Optimum growth temperature (°C)	T_m (°C)	Hphob _{K&D}	% Sequence ID
4el8	<i>C. bescii</i>	75	80	140.4	100
111y	<i>C. thermocellum</i>	60	65 ^a [8]	141.7	62.7
4jji	<i>T. fusca</i>	55	65	135.3	54.7
5cvy	<i>B. pumilus</i>	30	45	127.7	46.4
1f9d	<i>C. cellulolyticum</i>	34	37 ^a [9]	120.2	61.9

^a Indicates optimal operating temperature



Can activity and thermostability be explained by direct structural comparisons?

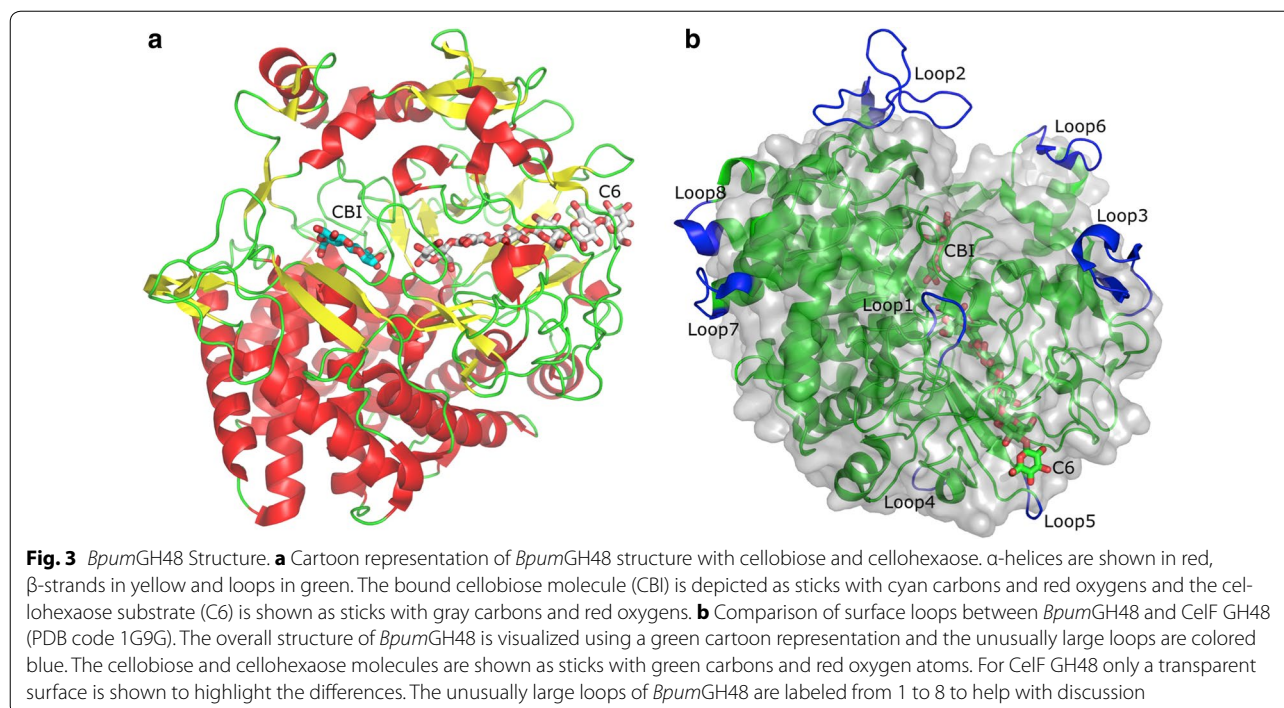
Pair-wise secondary structure matching of structures with at least 70% secondary structure similarity by PDBeFold [11] found 36 unique structural matches for *Bpum*GH48 from the protein data bank. Most of these were different structures of CelS [12] or CelF [13]. After discarding different variants and mutants of the same protein, only six unique entries could be found. Out of these, CelF is most similar. *Bpum*GH48 has 51% sequence similarity and 77% secondary structure similarity with CelF (PDB code 1G9G). The C_{α} root mean square deviations of all compared structures varied between 0.91 and 1.02 Å showing that the overall backbone of all of the known GH48 structures is similar.

All GH48 domains have $(\alpha/\alpha)_6$ barrel fold (Fig. 3a) with nearly identical organization of the active site tunnel. The tunnel layout is depicted in great details in [6] and [10]. What is remarkable is the conservation of the tunnel structure throughout the five GH48s considered in this study. Out of 36 residues that represent the tunnel walls and contact with the substrate/product, 27 are universally conserved and most of the rest are highly conserved (Table 2). We believe that this highly conserved substrate-binding tunnel is the main explanation for the similar levels of activity shown by different GH48s.

The most unique feature about the structure of *Bpum*GH48 is the eight unusually long peptide inserts that result in extra loops on the surface of the molecule when compared to other GH48 enzymes (Fig. 3b). Beyond these loops, the core structure is very similar to other well described GH48 enzymes, such as CelF GH48 [13], CelS GH48 [12], or *T. fusca* GH48 [3]. Compared to CelF GH48, *Bpum*GH48 has 80 more residues between Ser2 and Leu702 when the two structures are superimposed. Loop 5 (Leu303 to Asn308) is located near the tunnel entrance and loops 2 (Arg463 to Ala493) and 6 (Phe664 to Gly674) are near the exit. Due to their position, these loops have the potential to affect substrate-binding and product expulsion. Although, computer simulations indicate that the *Bpum*GH48 loops near the tunnel exit do not affect product inhibition [5]. However, they could be one of the reasons for the lower thermostability of *Bpum*GH48 by being more exposed to solvent. Without extensive mutational experiments, we are not able to deduce a clear role for them.

More detailed comparisons are necessary to explain thermostability and potentially activity

The GH48 enzymes evaluated here represent a wide range of thermostability within this family, covering melting temperatures from 37 to 80 °C. More detailed comparisons of the X-ray crystal structures allow us to evaluate and compare these GH48 family members to identify features contributing to differences in stability or activity. Previous research from our group comparing mesophilic and thermophilic enzymes determined that the quality of amino acid side-chain packing is often improved in thermophilic enzymes compared to mesophilic homologues [14]. Even though this work suggests thermophilic enzymes cannot tolerate imperfections, such as poor side-chain packing, some mesophilic homologues display similarly optimized side-chain packing suggesting alternative mechanisms must be responsible for differences in thermostability. Here, we applied the same analysis, comparing the atomic packing, or side-chain packing, for clusters of interacting residues throughout the core of the proteins. We compared the



most thermostable family member, the GH48 from *C. bescii*, to each of the other family members. A negative $\Delta\text{SASA}_{1,4}$ (Solvent Accessible Surface Area) indicates the *C. bescii* enzyme cluster displays smaller and/or fewer cavities, demonstrating improved atomic packing compared to the corresponding cluster from the other GH48 family member. We find that among the 5 GH48 enzymes all display comparable and optimized side-chain packing (Fig. 4).

The hydrophobic effect drives protein folding and hydrophobic interactions often contribute significantly to protein binding affinity [15]. Removing a buried methylene or methyl group can destabilize a protein, with examples showing destabilization of more than 1 kcal/mol [15, 16]. Alternatively, introducing new methylene groups can stabilize a protein, presenting a mechanism that protein design algorithms have used to rationally increase the thermostability by identifying positions that can accommodate larger hydrophobic amino acids [13, 15, 16, 27]. Here, we compare the hydrophobicity of the protein core regions for each GH48 family member from Table 1. Scores comparing the hydrophobicity of the twenty amino acids were developed based on the idea that protein unfolding would transfer hydrophobic residues to the aqueous solvent environment, a process which is energetically unfavorable [17]. Using the amino acid hydrophobicity scale of Kyte and Doolittle, we see that the hydrophobic score ($\text{Hphob}_{\text{K\&D}}$ in Table 1) correlates with the T_m of each GH48 enzyme (Table 1) with

more thermostable GH48 family members having higher $\text{Hphob}_{\text{K\&D}}$ scores [17]. The total hydrophobicity scores for each GH48 family member can change and may not be representative of overall stability. Therefore, we conducted a more detailed analysis by comparing the hydrophobicity for each cluster of interacting residues, as was done to compare differences in side-chain packing ($\Delta\text{SASA}_{1,4}$) in Fig. 4. We compared the most thermostable family member, the GH48 from *C. bescii*, to each of the other family members. $\Delta\text{Hydrophobicity}$ represents the differences between the $\text{Hphob}_{\text{K\&D}}$ scores for each of the *C. bescii* GH48 residue clusters across GH48 family members. Positive $\Delta\text{Hydrophobicity}$ values represent *C. bescii* clusters that are more hydrophobic compared to the corresponding clusters in other family members. *C. bescii* GH48 has a great number of clusters that are more hydrophobic, indicating increased buried hydrophobicity, which may explain the difference in stability between the *C. bescii* GH48 and other less thermostable family members (Fig. 5).

When considering the overall activity of these proteins, given that the catalytic residues are identical and the catalytic tunnel residues are highly conserved, we have examined the SASA, which may explain what we believe to be responsible for their similar activity. We note that all of the structures are uniformly well packed, mostly equally across the family members that we evaluated. This result indicates that there should be an equivalent freedom of motion within the core of each enzyme and

Table 2 Highly conserved tunnel-forming residues of GH48s

<i>B. pumilus</i>	<i>C. bescii</i>	<i>T. fusca</i>	<i>C. thermocellum</i>	<i>C. cellulolyticum</i>
His30	His	His	His	His
Glu38	Glu	Glu	Glu	Glu
Ala39	Ala	Ala	Ala	Ala
Glu49	Glu	Glu	Glu	Glu
Thr106	Thr	Thr	Thr	Thr
Ala108	Ala	Ile	Ala	Ala
Leu121	Leu	Leu	Leu	Leu
Trp150	Trp	Trp	Trp	Trp
Asn174	Asn	Asn	Asn	Asn
Phe176	Phe	Tyr	Phe	Phe
Gln177	Gln	Gln	Gln	Gln
Thr210	Ile	Thr	Thr	Thr
Glu212	Asp	Asp	Asp	Asp
Gln214	Asn	Asn	Ser	Gly
Gln219	Gln	Gln	Gln	Gln
Arg221	Arg	Arg	Arg	Lys
Thr223	Thr	Thr	Thr	Thr
Asp227	Asp	Asp	Asp	Asp
Lys267	Lys	Lys	Lys	Lys
Tyr268	Tyr	Tyr	Tyr	Tyr
Trp295	Trp	Trp	Trp	Trp
Tyr296	Tyr	Tyr	Tyr	Tyr
Ser298	Ala	Ser	Ala	Ala
Trp309	Trp	Trp	Trp	Trp
Trp311	Trp	Trp	Trp	Trp
Ile313	Ile	Ile	Ile	Ile
Tyr322	Tyr	Tyr	Tyr	Tyr
Tyr403	Tyr	Trp	Tyr	Tyr
Trp411	Trp	Trp	Trp	Trp
Met414	Phe	Phe	Phe	Met
Trp417	Trp	Trp	Trp	Trp
Asp534	Asp	Asp	Asp	Asp
Glu590	Glu	Glu	Glu	Glu
Arg592	Arg	Pro	Arg	Arg
Arg682	Arg	Arg	Arg	Arg
Trp684	Trp	Trp	Trp	Trp

Non-conserved residues are shown in bold font

this could explain the lack of kinetic differences between these enzymes, as we have observed roughly similar activities for them.

Conclusions

We have utilized classical biochemistry approaches to study three different family 48 glycoside hydrolases, which display widely different temperature optima. Additionally, we used X-ray crystallography and

computational analyses to explain the difference (or lack thereof) between cellulolytic activity and thermostability. To summarize, we have demonstrated that the three GH48 exoglucanases tested have very different melting temperatures despite having high sequence identity and similar enzymatic activity. Based on sequence and structural alignments as well as the molecular modeling, we conclude that some of these differences lay in the loop regions of these proteins but also in differences in the hydrophobic clusters within the proteins. If these explanations are correct, we may be able to modify the temperature optima of GH48 exoglucanases in the future. Additionally, they may be examples of how thermostability is modulated in other enzymes.

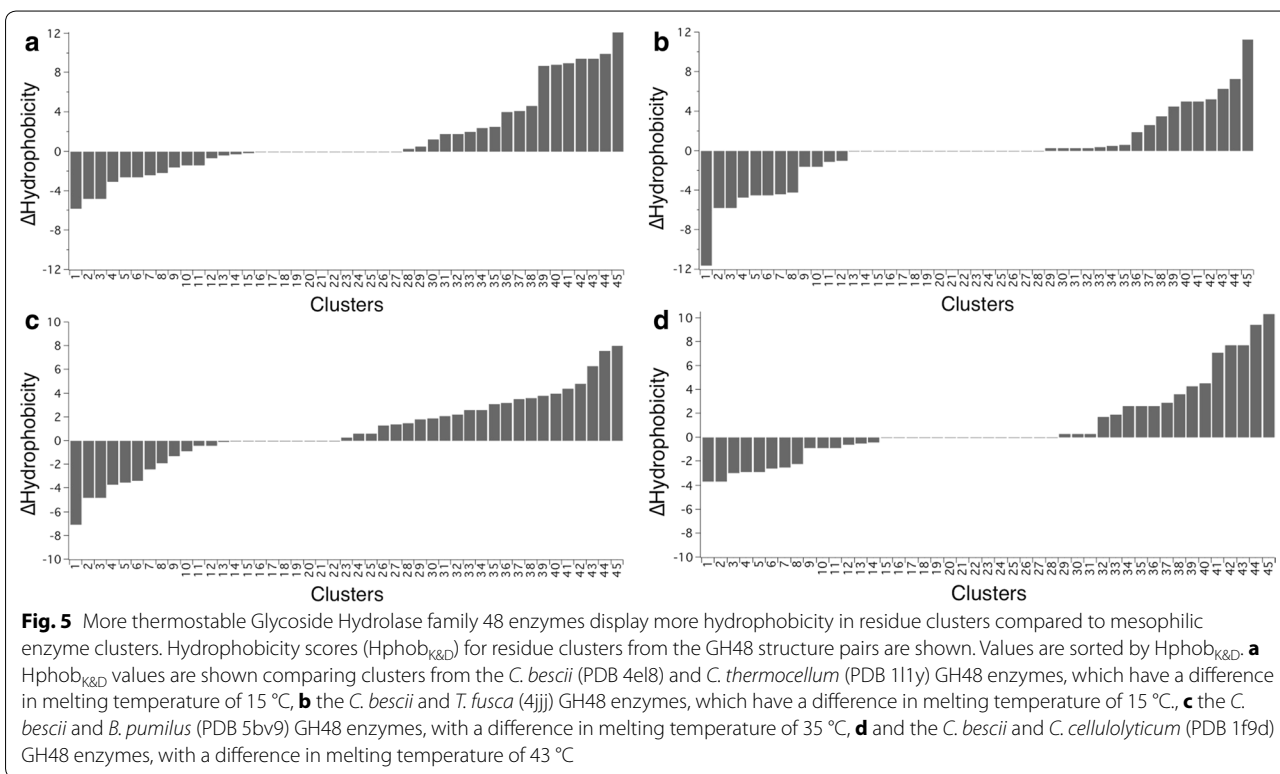
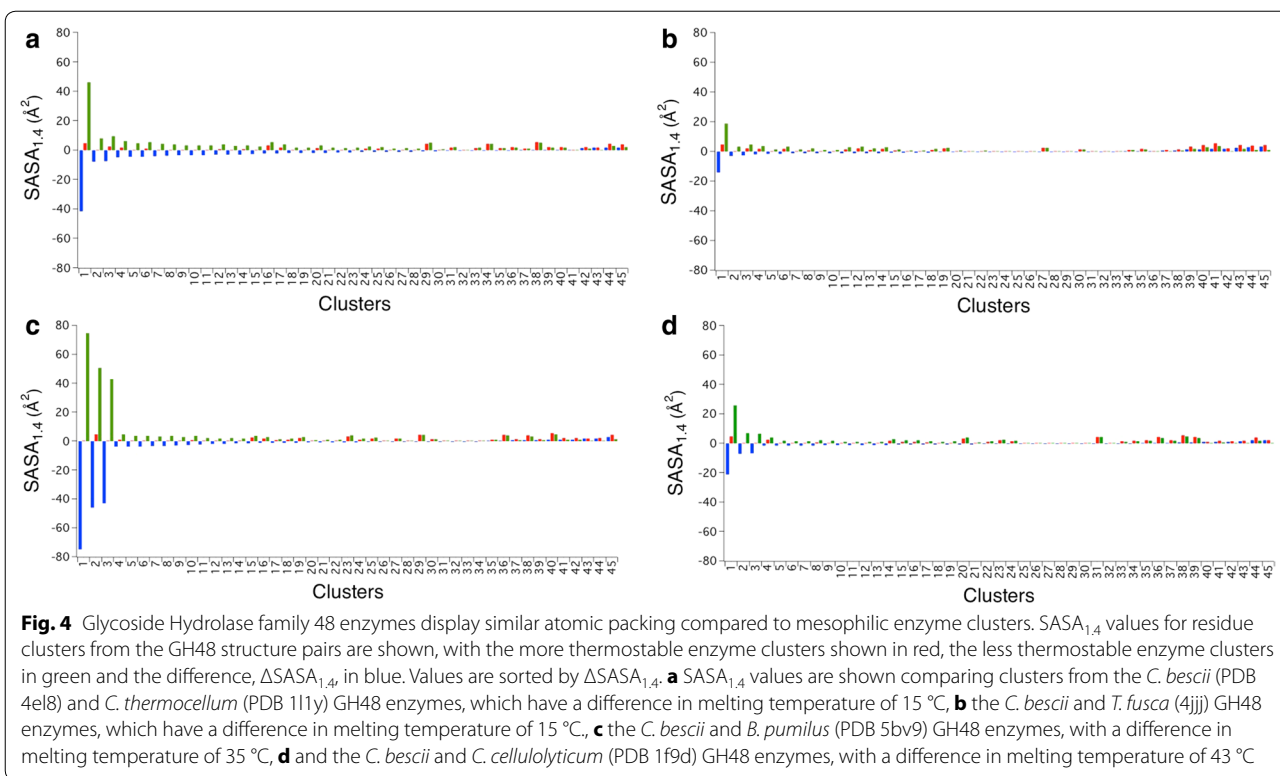
Methods

Cloning, overexpression, and purification of CelA CBM3-GH48 isolated from *C. bescii*

Cloning, overexpression, and purification of CelA CBM3-GH48 isolated from *C. bescii*: PCR fragment of CBM3-GH48 was made by two primers F-CBM3v-*NheI* of ACACCGGCTAGCAGCAGCACACCTGTAGCAGG and R-GH48-*XhoI* of TAGCTTCTCGAGTTATTGATTGCCAAACAGTA, and its template was the *C. bescii* genomic DNA. The PCR fragment was inserted into pET28a with *NheI* and *XhoI*. The correct insert was verified by DNA sequencing. Plasmid with the target gene was overexpressed in *E. coli* BL21 (DE3) strain (Ipswich, MA, USA). The gene expression was induced by 0.3 IPTG under 16 °C. The cells were harvested and lysed by sonication, and was purified by Nickel-NTA (Invitrogen, Grand Island, NY, USA). The affinity purified protein was further purified using hydrophobic interaction chromatography using a Source 15 phenyl resin column (GE) and 20 mM Acetate pH5 1 M ammonium sulfate buffer followed by size exclusion chromatography (SEC) using a Superdex 75 column using 20 mM Acetate pH5 100 mM NaCl.

Cloning, overexpression, and purification of *B. pumilus* GH48

The *B. pumilus* GH48 construct was synthesized and codon optimized for *E. coli* expression and placed in a pMal (NEB) MBP expression vector with a Genase cleavage site. The plasmid with the target gene was overexpressed in *E. coli* BL-21(DE3), induced with 0.3 mM IPTG and induced for 21 h at 17 °C. Cells were pelleted at 10,000×g and re-suspended in 40 mL Bugbuster (EDM Millipore) with C-Complete protease inhibitor (Sigma) and then sonicated for one min and allowed to incubate for at RT for one h. Cell debris was then pelleted by centrifugation at 10,000×g and the remaining supernatant was added to buffer-equilibrated amylose beads and



incubated for one h and then washed with 20 mM Tris buffer pH 7.4 with 200 mM NaCl. The protein was then released from the beads with Genesee I.

The resultant mix of maltose binding protein (MBP), MBP fusion, and cleaved GH48 then was then separated by SEC to separate the MBP and then further purified using anion exchange chromatography (AEC) with a Source 15Q column pH 6.8 Tris buffer with 2 M NaCl. Finally, hydrophobic interaction chromatography (HIC) using a Source 15-phe column (GE) with 20 mM pH 5.0 acetate buffer and a 1 M ammonium sulfate gradient.

***T. fusca* GH48**

T. fusca GH48 was provided by David Wilson's laboratory and produced as described in [7].

Circular dichroism (CD)

CD measurements were carried out using a Jasco J-715 spectropolarimeter with a jacketed quartz cell with a 1.0 mm path length. The cell temperature was controlled to within ± 0.1 °C by circulating 90% ethylene glycol using a Neslab R-111 m water bath (NESLAB Instruments, Portsmouth, NH, U.S.A.) through the CD cell jacket. The results were expressed as mean residue ellipticity $[\theta]_{\text{mrv}}$. The spectra obtained were averages of five scans. The spectra were smoothed using an internal algorithm in the Jasco software package, J-715 for Windows. Protein samples were studied in 20 mM sodium acetate buffer, pH 5.0 with 100 mM NaCl at a protein concentration of 0.35 mg/mL for the near UV CD. Thermal denaturation of different constructs was monitored by CD in the near UV (190–260 nm) region. For the analysis of thermostability, the temperature was increased from 55 to 105 °C with a step size of 0.2 °C, and monitored at a wavelength of 222 nm.

Enzyme digestions

The GH48 enzymes were loaded at a concentration of 20 mg protein per g glucan to 1.5% w/w solutions of phosphoric acid swollen cellulose (PASC) and bacterial microcrystalline cellulose (BMCC). Bacterial microcrystalline cellulose (BMCC) was prepared from BC as described previously [18]. Assays were carried out at 75, 60, and 37 °C in 20 mM acetate buffer, pH 5.5 containing 10 mM CaCl_2 , and 100 mM NaCl. Digestion assays were performed in triplicate, and the final glucose concentration was determined using HPLC. To measure cellulose conversion, 60 μL of each hydrolysate sample was diluted tenfold and filtered using a 0.45 μm filter. Glucose concentrations were measured by HPLC (Agilent) using an Aminex HPX-87H column (BioRad Laboratories) using a 5 mM sulfuric acid mobile phase and a flow rate of 0.6 mL/min. The sample injection volume

was 20 μL and the run time was 11 min. For sugar product determination, digestion aliquots were analyzed using an ICS-5000+ System (ThermoFisher Scientific) equipped with a CarboPac PA20 column/guard column and pulsed amperometric detection (PAD). Monomeric sugars and xylobiose were eluted at 0.45 mL/min using an isocratic eluent concentration of 32.5 mM NaOH. The carbohydrate (quad potential) waveform for an Ag/AgCl reference electrode was used for detection and quantitation. The glucose concentration from each reaction was divided by the maximal glucose yield obtained from compositional analysis, in order to calculate a fractional glucan conversion for each reaction.

Crystallization

BpumGH48 crystals in complex with cellobiose (*BpumGH48-C2*) and cellobiose/cellohexaose (*BpumGH48-C2C6*) were initially obtained with sitting drop vapor diffusion using a 96-well plate with Grid Screen Salt HT from Hampton Research (Aliso Viejo, CA). 50 μL of well solution was added to the reservoir and drops were made with 0.2 μL of well solution and 0.2 μL of protein solution using a Phoenix crystallization robot (Art Robbins Instruments, Sunnyvale, CA). The crystals were grown at 20 °C using screens containing 1–3 M malonate with pH 5–7 and 20 mM cellobiose. The protein solutions contained 15 mg/mL of protein in 20 mM acetate buffer pH 5, with 100 mM NaCl and 10 mM CaCl_2 . Before freezing crystals were briefly soaked in a drop containing excess amounts of cellohexaose, 10% (v/v) glycerol and 10% (v/v) ethylene glycol.

Data collection and processing

The *BpumGH48* crystals were flash frozen in a nitrogen gas stream at 100 K before home source data collection using an in-house Bruker X8 MicroStar X-Ray generator with Helios mirrors and Bruker Platinum 135 CCD detector. Data were indexed and processed with the Bruker Suite of programs version 2014.9 (Bruker AXS, Madison, WI).

Structure solution and refinement

Intensities were converted into structure factors and 5% of the reflections were flagged for R_{free} calculations using programs F2MTZ, Truncate, CAD, and Unique from the CCP4 package of programs [19]. The program MOLREP [20] version 11.2.08 was used for molecular replacement using the unliganded structure of a family 48 glycoside hydrolase from *C. bescii* (PDB entry 4EL8 [10]) as the search model. Refinement and manual correction was performed using REFMAC5 [21] version 5.8.135 and Coot [22] version 0.8.2. The MOLPROBITY method [23] was used to analyze the Ramachandran plot and root mean

square deviations (rmsd) of bond lengths and angles were calculated from ideal values of Engh and Huber stereochemical parameters [24]. Wilson B-factor was calculated using CTRUNCATE version 1.15.10 [19]. The data collection and refinement statistics are shown in Table 1.

The structure of *BpumGH48-C2C6* with cellobiose and cellohexaose was refined to a resolution of 2.0 Å with R and R_{free} of 0.146 and 0.189, respectively. There is one molecule in the asymmetric unit with a cellobiose and a cellohexaose molecule (Fig. 3). It has an (alpha/alpha)₆ barrel fold with several malonate, ethylene glycol, and glycerol molecules on the surface. This structure has been deposited in the Protein Data Bank (PDB) with code 5CVY. The structure of *BpumGH48-C2* with cellobiose (PDB code 5BV9) was solved at resolution 1.93 Å and R and R_{free} of 0.161 and 0.207, respectively. X-ray data collection and refinement statistics and details are listed in Additional file 1: Table S1.

Structure analysis

Programs Coot [22], PyMOL (<http://www.pymol.org>) and ICM (<http://www.molsoft.com>) were used for comparing and analyzing structures. Figure 3 was created using PyMOL.

Protein sequence analysis

Sequences were aligned and analyzed using the MacVector software (MacVector, Inc., Cary, NC) [25]. Sequence alignments were performed using the GONNET substitution matrix [26], with a gap opening penalty of 10 and a gap extension penalty of 0.05.

Identification of residue clusters

Residue clusters were determined as previously described [14]. Briefly, interacting residues were identified using a distance cutoff of 3 Å between side-chain heavy atoms (C, N, O and S) using the protein design software, Rosetta [27, 28]. Structurally equivalent residue clusters in homologous mesophilic enzymes were identified using the structural alignment algorithm, jFatCat flexible [29]. Residue clusters were filtered based on degree of solvent accessibility, selecting only clusters where each residue displayed less than 3 Å² of SASA as determined using Naccess [30].

Comparing structurally equivalent residue clusters

The residue accessible surface areas were computed using the program Naccess. Naccess rolls a probe of a given radius over the van der Waals surface of a molecule to trace the accessible surface. A probe of radius 1.4 Å was used here to reflect the radius of water and thus the solvent accessible surface area. Graphs were generated using IGOR Pro (WaveMetrics Inc., Lake Oswego, OR).

Additional file

Additional file 1. Additional table and figure.

Authors' contributions

RB: purified the GH48 proteins, and performed the enzyme digestions, as well as the CD experiments, he participated in the design of the study and was a major contributor in writing of the manuscript. DS: Performed the simulations and contributed to writing of the manuscript. MA: Performed the X-ray crystallography and analysis and contributed to the writing of the manuscript. QX: Performed the requisite molecular biology to transform the cells, expressed the proteins, and contributed to the writing of the manuscript. MC: Helped design the study and participated in the writing of the manuscript. JB: Helped design the study and participated in the writing of the manuscript. MH: Helped design the study, supervised the work, and wrote the manuscript. YB: Helped design the study, supervised the work, and wrote the manuscript. VW: Performed the X-ray crystallography and analysis. All authors read and approved the final manuscript.

Author details

¹ Biosciences Center, National Renewable Energy Laboratory, 15013 Denver West Parkway, Golden, CO 80401, USA. ² Department of Food Science, Cornell University, Ithaca, NY, USA. ³ Biochemistry, Molecular and Cell Biology, Cornell University, Ithaca, NY, USA.

Acknowledgements

We would like to acknowledge Edward Bayer for providing the bacterial microcrystalline cellulose.

Competing interests

The authors declare that they have no competing interests.

Declarations

All authors consent to the publication. All data generated or analyzed during this study are included in this published article [and its additional files]. The structure of *BpumGH48-C2C6* has been deposited in the Protein Data Bank (PDB) with code 5CVY, <http://www.rcsb.org/pdb/explore/explore.do?structureId=5CVY>.

Funding

This work was supported by the BioEnergy Science Center (BESC). BESC is a U.S. Department of Energy Bioenergy Research Center supported by the Office of Biological and Environmental Research in the U.S. DOE Office of Science.

Publisher's Note

Springer Nature remains neutral with regard to jurisdictional claims in published maps and institutional affiliations.

Received: 11 July 2017 Accepted: 2 November 2017

Published online: 30 November 2017

References

1. Sukharnikov LO, et al. Sequence, structure, and evolution of cellulases in glycoside hydrolase family 48. *J Biol Chem*. 2012;287:41068–77.
2. Lombard V, Golaconda Ramulu H, Drula E, Coutinho PM, Henrissat B. The carbohydrate-active enzymes database (CAZy) in 2013. *Nucleic Acids Res*. 2014;42:D490–5.
3. Kostylev M, et al. Cel48A from *Thermobifida fusca*: structure and site directed mutagenesis of key residues. *Biotechnol Bioeng*. 2014;111:664–73.
4. Berger E, Zhang D, Zverlov VV, Schwarz WH. Two noncellulosomal cellulases of *Clostridium thermocellum*, Cel9I and Cel48Y, hydrolyse crystalline cellulose synergistically. *FEMS Microbiol Lett*. 2007;268:194–201.

5. Chen M, et al. Strategies to reduce end-product inhibition in family 48 glycoside hydrolases. *Proteins Struct Funct Bioinf*. 2016;84:295–304.
6. Parsiegla G, Reverbel C, Tardif C, Driguez H, Haser R. Structures of mutants of cellulase Cel48F of *Clostridium cellulolyticum* in complex with long hemithiocellooligosaccharides give rise to a new view of the substrate pathway during processive action. *J Mol Biol*. 2008;375:499–510.
7. Irwin DC, Zhang S, Wilson DB. Cloning, expression and characterization of a family 48 exocellulase, Cel48A, from *Thermobifida fusca*. *Eur J Biochem*. 2000;267:4988–97.
8. <http://www.nzytech.com/products-services/cellulases/cz0115>. Accessed 10 Jan 2016.
9. <http://www.nzytech.com/products-services/cellobiohydrolases/cz0017>. Accessed 10 Jan 2016.
10. Brunecky R, et al. Revealing nature's cellulase diversity: the digestion mechanism of *Caldicellulosiruptor bescii* CelA. *Science*. 2013;342:1513–6.
11. Krissinel E, Henrick K. Secondary-structure matching (SSM), a new tool for fast protein structure alignment in three dimensions. *Acta Crystallogr Sect D*. 2004;60:2256–68.
12. Guimaraes BG, Souchon H, Lytle BL, David Wu JH, Alzari PM. The crystal structure and catalytic mechanism of cellobiohydrolase Cel5, the major enzymatic component of the *Clostridium thermocellum* Cellulosome. *J Mol Biol*. 2002;320:587–96.
13. Parsiegla G, et al. The crystal structure of the processive endocellulase CelF of *Clostridium cellulolyticum* in complex with a thiooligosaccharide inhibitor at 2.0 Å resolution. *EMBO J*. 1998;17:5551–62.
14. Sammond DW, et al. Comparing residue clusters from thermophilic and mesophilic enzymes reveals adaptive mechanisms. *PLoS ONE*. 2016;11:e0145848.
15. Pace CN, Shirley BA, McNutt M, Gajiwala K. Forces contributing to the conformational stability of proteins. *FASEB J*. 1996;10:75–83.
16. Takano K, Yamagata Y, Fujii S, Yutani K. Contribution of the hydrophobic effect to the stability of human lysozyme: calorimetric studies and X-ray structural analyses of the nine valine to alanine mutants. *Biochemistry*. 1997;36:688–98.
17. Kyte J, Doolittle RF. A simple method for displaying the hydropathic character of a protein. *J Mol Biol*. 1982;157:105–32.
18. Valjamae P, Sild V, Nutt A, Pettersson G, Johansson G. Acid hydrolysis of bacterial cellulose reveals different modes of synergistic action between cellobiohydrolase I and endoglucanase I. *Eur J Biochem*. 1999;266:327–34.
19. Winn MD, et al. Overview of the CCP4 suite and current developments. *Acta Crystallogr D Biol Crystallogr*. 2011;67:235–42.
20. Vagin A, Teplyakov A. Molecular replacement with MOLREP. *Acta Crystallogr D Biol Crystallogr*. 2010;66:22–5.
21. Murshudov GN, et al. REFMAC5 for the refinement of macromolecular crystal structures. *Acta Crystallogr D Biol Crystallogr*. 2011;67:355–67.
22. Emsley P, Lohkamp B, Scott WG, Cowtan K. Features and development of coot. *Acta Crystallogr D Biol Crystallogr*. 2010;66:486–501.
23. Chen VB, et al. MolProbity: all-atom structure validation for macromolecular crystallography. *Acta Crystallogr D Biol Crystallogr*. 2010;66:12–21.
24. Engh RA, Huber R. Accurate bond and angle parameters for X-ray protein-structure refinement. *Acta Crystallogr Sect A*. 1991;47:392–400.
25. Rastogi PA. MacVector. Integrated sequence analysis for the Macintosh. *Methods Mol Biol*. 2000;132:47–69.
26. Gonnet GH, Cohen MA, Benner SA. Exhaustive matching of the entire protein sequence database. *Science*. 1992;256:1443–5.
27. Kaufmann KW, Lemmon GH, Deluca SL, Sheehan JH, Meiler J. Practically useful: what the Rosetta protein modeling suite can do for you. *Biochemistry*. 2010;49:2987–98.
28. Kuhlman B, Baker D. Native protein sequences are close to optimal for their structures. *Proc Natl Acad Sci USA*. 2000;97:10383–8.
29. Ye Y, Godzik A. Flexible structure alignment by chaining aligned fragment pairs allowing twists. *Bioinformatics*. 2003;19(Suppl 2):ii246–55.
30. Hubbard SJ, Thornton JM. University of College London, 1993.

Submit your next manuscript to BioMed Central and we will help you at every step:

- We accept pre-submission inquiries
- Our selector tool helps you to find the most relevant journal
- We provide round the clock customer support
- Convenient online submission
- Thorough peer review
- Inclusion in PubMed and all major indexing services
- Maximum visibility for your research

Submit your manuscript at
www.biomedcentral.com/submit

